Journal of Manufacturing Processes 57 (2020) 136–152

Contents lists available at ScienceDirect

Journal of Manufacturing Processes

journal homepage: www.elsevier.com/locate/manpro

Experimental study on the effects of cold chamber die casting parameters on high-speed drilling machinability of casted AZ91 alloy

Şakir Yazman[a], Uğur Köklü[b,*], Levent Urtekin[c], Sezer Morkavuk[b], Lokman Gemi[d]

[a] Ilgın Vocational School, Selçuk University, 42615, Konya, Turkey
[b] Department of Mechanical Engineering, Karamanoglu Mehmetbey University, 70100, Karaman, Turkey
[c] Department of Mechanical Engineering, Ahi Evran University, 40100 Kırşehir, Turkey
[d] Meram Vocational School, Necmettin Erbakan University, 42000, Konya, Turkey

ARTICLE INFO

Keywords:
Cold chamber die casting
AZ91
High-speed drilling
Thrust force
Tool wear
Chip
Burr

ABSTRACT

In this study, the effects of the cold chamber die casting parameters on high-speed drilling machinability of AZ91 Magnesium alloys were experimentally investigated. The influence of different casting parameters (casting temperature, molding pressure, and gate speed) on microstructure, mechanical properties and machinability characteristics (thrust force, tool wear, built-up edge, built-up layer formation, surface topography, chip morphology, and burr formation) were examined. The experimental results showed that the grain size of the conventional casting sample was around 50 microns, while in other cold chamber die casting tests, it varied depending on temperature, pressure, and gate speed. It was observed that the tensile strength values of the samples produced with 1000 bar mold pressure were higher than those of other samples. In the formation of thrust force, the feed rate is more effective than the cutting speed. The least tool wear occurred in the drilling of the As-cast sample, while the highest tool wear occurred in the drilling of the sample which was produced with low pressure and low gate speed combination. As a result of the drilling tests, depending on casting and cutting parameters, three different types of chips were formed: fan, spiral cone, and long ribbon type. Furthermore, uniform and transient burrs in different sizes were observed.

1. Introduction

Magnesium (Mg) alloys are an excellent alternative for many engineering materials in industries due to their low density. For example, magnesium alloys are extensively used in the transportation sector to reduce fuel consumption and increase efficiency. These alloys are also used in biomedical applications and manufacturing of electronic products, nevertheless, the automotive industry is considered to be the largest consumer of magnesium alloys [1–4]. They are utilized in the manufacturing of many automotive parts, from engine components to car seat frames. Die casting is the most widely used production method of magnesium alloy automotive parts since it provides good production efficiency and near-net-shape parts which need minimal chip removal process [5,6]. In case inappropriate casting parameters are used, material defects such as jetting and porosity may occur. These defects reduce the strength, heat treatment capability, and weldability of the manufactured material. Although parts manufactured by the die casting method require minimal or no machining, drilling operation is almost inevitable for assembly of the components. It was stated that magnesium alloys have good machinability but fine chips removed during high-speed dry machining tend to self- ignition [7]. Also, due to the low melting temperature of magnesium alloys, built-up-edge is formed and this reduces surface quality and machining precision [8].

Machinability of AZ91 magnesium alloys has been investigated by many researchers. In these publications, drilling [9–15], turning [16–19], and milling [20,21] performance of the magnesium alloys were investigated. On the other hand, there is a limited number of works focused on high-speed machining of AZ91 magnesium alloys and the majority of these works, high-speed milling performance of magnesium alloys were investigated. In these papers, chip ignition and safety in machining [22–24], cutting forces [25], surface roughness [26], and tool wear [27] were studied. However, high-speed drilling of magnesium alloys has not been investigated adequately and there is a gap in the literature concerning this subject.

The studies on drilling of AZ91 magnesium alloy generally concentrated on the influence of cutting tool (cutting geometry, coating,

* Corresponding author.
E-mail addresses: syazman@selcuk.edu.tr (Ş. Yazman), ugurkoklu@gmail.com (U. Köklü), levent.urtekin@ahievran.edu.tr (L. Urtekin), sezermorkavuk@kmu.edu.tr (S. Morkavuk), lgemi@erbakan.edu.tr (L. Gemi).

https://doi.org/10.1016/j.jmapro.2020.05.050
Received 21 February 2020; Received in revised form 13 May 2020; Accepted 26 May 2020
Available online 24 June 2020

Table 1
Summary of previous studies on drilling of AZ91 magnesium alloys.

Materials	Machining conditions Cutting parameters	Research object	Ref.
AZ91E alloy (As cast)	*v: 35–188 m/min* *f: 0.22 mm/rev* *d:10 mm HSS twist drill* *Dry cutting*	Cutting forces Chip morphology Dust production	[9]
UNS M11917 (AZ91D) alloys (As cast)	*v: 40 and 60 m/min* *f: 0.05 and 0.2 mm/rev* *d: 6 mm HSS twist drill* *Dry and MQL cutting*	Surface roughness	[10]
AZ91 alloy (As cast)	*v: 100–2500 rpm* *f: 0.10 − 0.25 mm/rev* *d: 6.35 mm NH-DLC coated and uncoated HSS twist drill* *Dry and MQL cutting*	Tool life Temperature Coefficient of friction Torque	[11]
AZ91D alloy (As cast)	*v: 2000, 2500 and 3000 rev/min* *f: 2.1, 0.2 and 0.3 mm/rev* *d: 8 mm uncoated HSS, uncoated carbide* *Dry cutting*	Surface roughness Diametric error Circularity error	[12]
AZ91 alloy (As cast)	*v: 31.4–125 m/min* *f: 0.025 − 0.2 mm/rev* *d: 5 mm, Aqua-coated solid carbide drills with 2- and 3-flute bits* *Dry cutting*	Cutting forces Chip morphology Tool wear	[13]
AZ31 and AZ91 alloys (As cast)	*v: 45, 235 and 450 rpm* *f: 10, 15 and 30 mm/min* *d: 6 mm HSS twist drill* *Dry cutting*	Cutting forces Chip morphology	[14]
AZ91 alloy (Die casting)	*v: 1000 and 8000 rpm* *f: 0.05 and 0.3 mm/rev* *d: 5 mm HSS twist drill* *Dry cutting*	Tool wear Chip morphology	[15]

v: cutting speed and spindle speed, *f*: feed rate, *d*: diameter of drill.

Table 2
Chemical compositions of the AZ91 magnesium alloy.

Chemical composition in mass %							
Mg	Al	Cu	Fe	Ni	Zn	Mn	Si
Bal.	9.21	0.002	0.0038	0.00085	0.45	0.17	0.016

Table 3
Cold chamber pressure die casting production parameters.

Specimens	Casting temperature (°C)	Molding pressure (bar)	Gate speed (m/s)
As-cast	–	–	–
PC-1	640	1200	45
PC-2	640	1200	60
PC-3	660	1000	45
PC-4	680	1000	30
PC-5	680	1000	60
PC-6	680	800	45

etc.), cutting environment (dry, minimum quantity lubrication (MQL)), and cutting parameters (cutting speed, feed rate) on machinability. These studies were summarized in Table 1.

Balout et al. [9] focused on the effects of workpiece temperature on dust generation, cutting forces, and chip morphology in dry drilling of 6061 and A356 Aluminum alloys, AZ91E magnesium alloy, and 70 − 30 brass. They found that the workpiece temperature significantly influenced dust production and stressed that lower material temperature causes to lower dust generation and reduces cutting forces. Wang et al. [15] presented a wear mechanism map for determining proper cutting parameters considering tool wear in drilling of die-cast AZ91 magnesium alloy using uncoated HSS drill. Bhowmick and Alpas [11] studied the performance of diamond-like carbon-coated HSS tool taking into consideration torque and temperature generation in minimum quantity water lubrication drilling of AZ91 magnesium alloy. They reported that rapid failure occurred in dry drilling due to adhesion of magnesium in case of the use of both HSS and diamond-like carbon-coated tools. Kayir [12] optimized cutting parameters such as cutting speed, feed rate, and tool material in drilling AZ91D magnesium alloy. The influence of cutting parameters on hole quality was investigated and results showed that cutting tool material had a great influence on surface roughness, while its impact on circularity was low. Ratna Sunil et al. [14] researched drilling machinability of AZ31 and AZ91 in order to determine the influence of aluminum (Al) content in magnesium alloys on machinability characteristics. They stated that Al content in the form of the secondary phase significantly changed machining characteristics by increasing cutting forces and providing discontinuous chips. Berzosa et al. [10] concentrated on tool selection in dry and MQL drilling of die-casted UNS M11917 magnesium alloy. Two different point angle drills were utilized and machinability was evaluated based on surface roughness. They reported that tools with 118° point angle presented better performance in higher cutting speeds but tools with 135° point angle were a btter choice for drilling at lower cutting speeds. Köklü et al. [13] investigated the influence of drill flute number on drilling

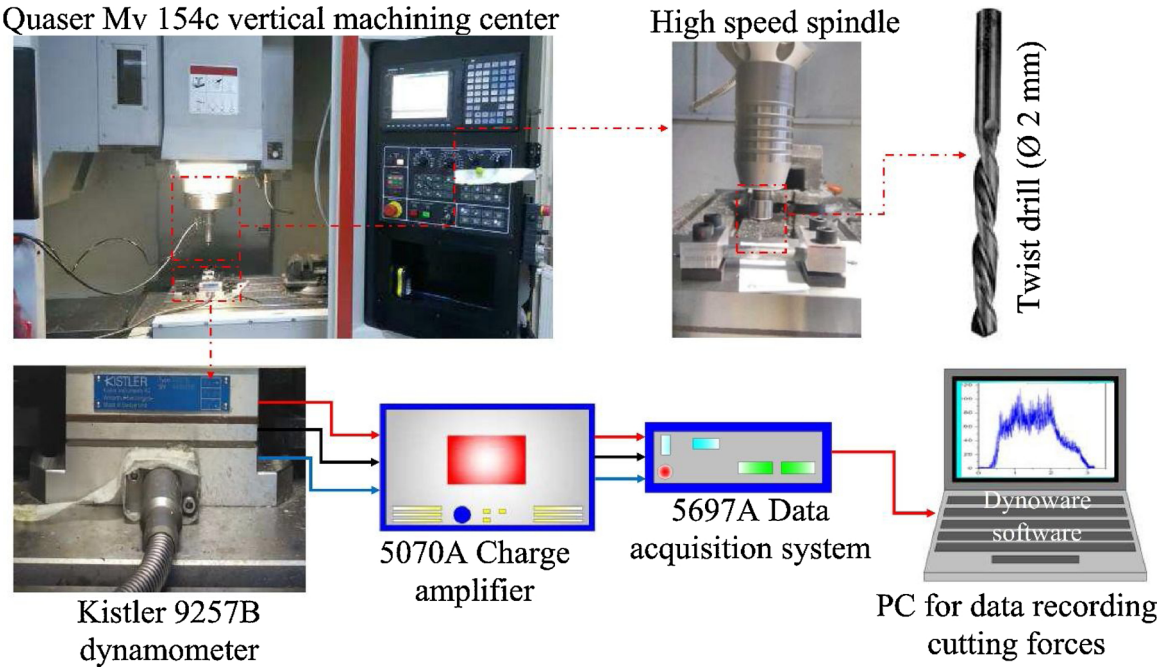

Fig. 1. Experimental setup.

Table 4
Drilling parameters.

Constant parameters	Variable parameters
Feed rate 100 mm/min	62.8 m/min (10,000 rpm) 157.1 m/min (25,000 rpm) 251.3 m/min (40,000 rpm)
Cutting speed 125.6 m/min (20,000 rpm)	150 mm/min 250 mm/min 350 mm/min

performance of casted AZ91 magnesium alloy considering thrust force, tool wear, tool life, chip morphology. Also, hardness and microstructures of borehole were examined. Results showed that flute numbers had a significant effect on drilling machinability of AZ91 and two fluted tools generated lower forces while less tool wear occurred on three fluted tools.

In previous works on drilling of AZ91 magnesium alloy, cutting parameters, cutting tools, and cutting environment were studied. The influence of casting parameters on high-speed drilling performance of casted AZ91 Mg alloy has not been investigated yet. In this comprehensive study, the effects of the cold chamber die casting parameters on microstructure, mechanical properties, and high-speed drilling machinability of die-casted AZ91 Mg alloys are investigated experimentally. The results of machining were correlated with the material production parameters.

2. Materials and methods

The samples used in this study were prepared from AZ91 material produced using both conventional casting and cold pressure die casting method.1600 kN metal press Mp 100 cold chamber die casting machine was utilized. The temperature of the fixed mold was 175 °C while moving mold temperature was 225 °C. In all tests, 0.25 % by volume of SF6 -Balance N_2 gas was used as a protective gas and the gas flow rate was 600 L/h. The chemical composition of the cast AZ91 magnesium alloy is shown in Table 2 [12].

The mechanical and metallographic properties of the samples were determined by tensile test and microstructure analysis of the parts produced with different casting parameters (casting temperature, molding pressure, and gate speed) by pressure casting method. Table 3 shows the cold press die casting parameters.

The uniaxial tensile tests of specimens in accordance with ASTM B557 M standard were carried out on a Shimadzu 100 kN tensile test machine. High-speed drilling tests were performed on Quaser MV154 C three-axis vertical machining center using no coolant. Fig. 1 illustrates the schematic setup of the drilling experiments. In the experimental study, a Sfida brushless high-speed spindle which has 60 000 rpm maximum spindle speed, 370 W power, and 8.82 cN m torque was used. Solid carbide drill bits with a 30° helix angle, 118° point angle, and 2 mm diameter were used. The dimensions of the drilling samples were W75 mm x H10 mm x T6 mm. The drilling time varies between 1.33 and 4.46 s depending on cutting parameters. A new drill bit was used for each experiment. A three-component piezo-electric dynamometer (Kistler 9257 B type), a charge amplifier, an A/D converter, and a computer with software were used for measurement of the thrust force. The specimens are rigidly clamped onto the dynamometer with the help of four bolts. After drilling tests, hole exits were examined using a Keyence VHX-900 digital microscope. Also, some holes were cross-sectioned into two parts along the radial axis and the borehole surface was analyzed using scanning electron microscopy (SEM). The surface roughness of the boreholes was determined using a non-contact type Zygo ZeGage optical profiler. The surface was scanned with a 20X mirau objective. Scan length in the Z direction was 150 μm while the scanned area was 417 μm x 417 μm. The cutting parameters used in the drilling tests are given in Table 4.

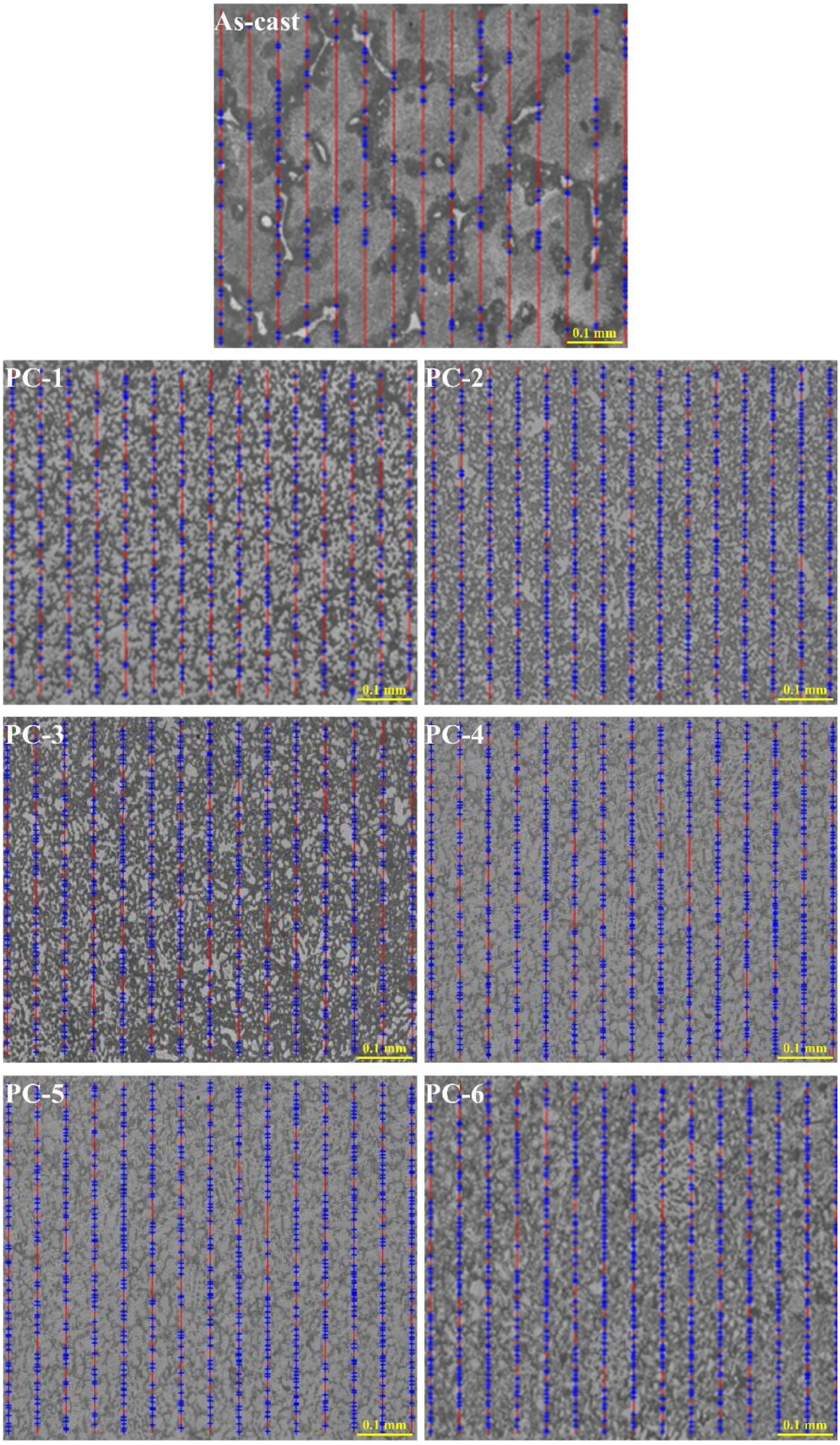

Fig. 2. Microstructure images (at 100X magnification) of specimens.

Table 5
ASTM grain size number, grain length and phase ratio obtained with an optical microscope.

Specimens	ASTM grain size number	Grain length (diameter, mm)	Phase ratio % α-Mg-$Mg_{17}Al_{12}$
As-cast	5.5	0.051	–
PC-1	9	0.015	63.6 – 36.4
PC-2	10	0.010	58 – 42
PC-3	9	0.015	54.9 – 45.1
PC-4	9.5	0.013	54.6 – 45.4
PC-5	10	0.010	60 – 40
PC-6	10	0.009	55 – 45

Table 6
Mechanical properties of cast and pressure die casting samples.

Specimens	Tensile stress (MPa)	Yield strength (MPa)	Elongation (%)	Toughness (kJ/m^3)
As-cast	169.2	68.4	3.87	4576
PC-1	173.6	93.7	2.32	2757
PC-2	168.5	76.8	2.88	3467
PC-3	205.1	106.2	4.60	7157
PC-4	221.5	105.6	6.26	10,725
PC-5	160.8	124.7	2.14	2448
PC-6	214.1	96.8	5.37	8763

3. Experimental results and discussions

3.1. Microstructure examinations

The samples were grinded using 120 – 320-1000 grit emery paper and then were polished. After the polishing process, the samples were etched using 2 mL of HNO_3-98 mL of methanol mixture for 2 – 10 sec. The microstructure of the specimens was monitored using an optical microscope at 100X magnification (Fig. 2).

As can be seen from Fig. 2, the grain structure of the samples produced by As-cast considerably differs from the structure of pressure casting samples. In the samples produced with cold pressure casting, the finer grain size was observed and it was determined that the optimum process parameters affected the mechanical properties. ASTM grain size, grain length, and phase ratio values of the specimens are given in Table 5. It is seen that the grain size of the classical casting sample is around 50 microns. While in cold chamber die casting tests, it is seen that grain size varies depending on temperature, pressure, and gate speed. It was found that the phase changes were α-Mg and $Mg_{17}Al_{12}$ and a balanced phase change affected the properties (Fig. 3).

3.2. Tensile test analysis

The tensile stress, yield stress, elongation, and toughness values obtained from the tensile tests of the samples are given in Table 6 and the stress-strain curve is given in Fig. 4. It can be seen that the strength values of PC-3, PC-4, and PC-6 samples are high. This result can be

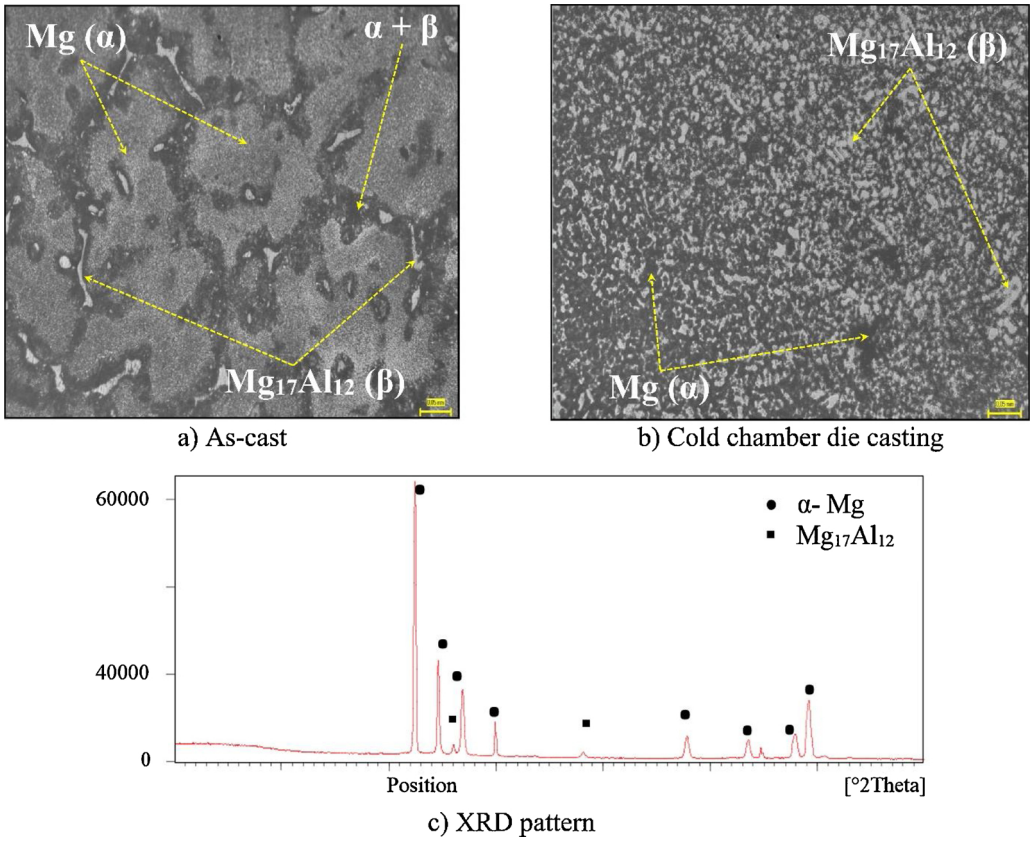

Fig. 3. a) α-Mg and $Mg_{17}Al_{12}$ phases in As-cast sample, b) cold chamber die casting sample, and c) XRD pattern of AZ91 casting.

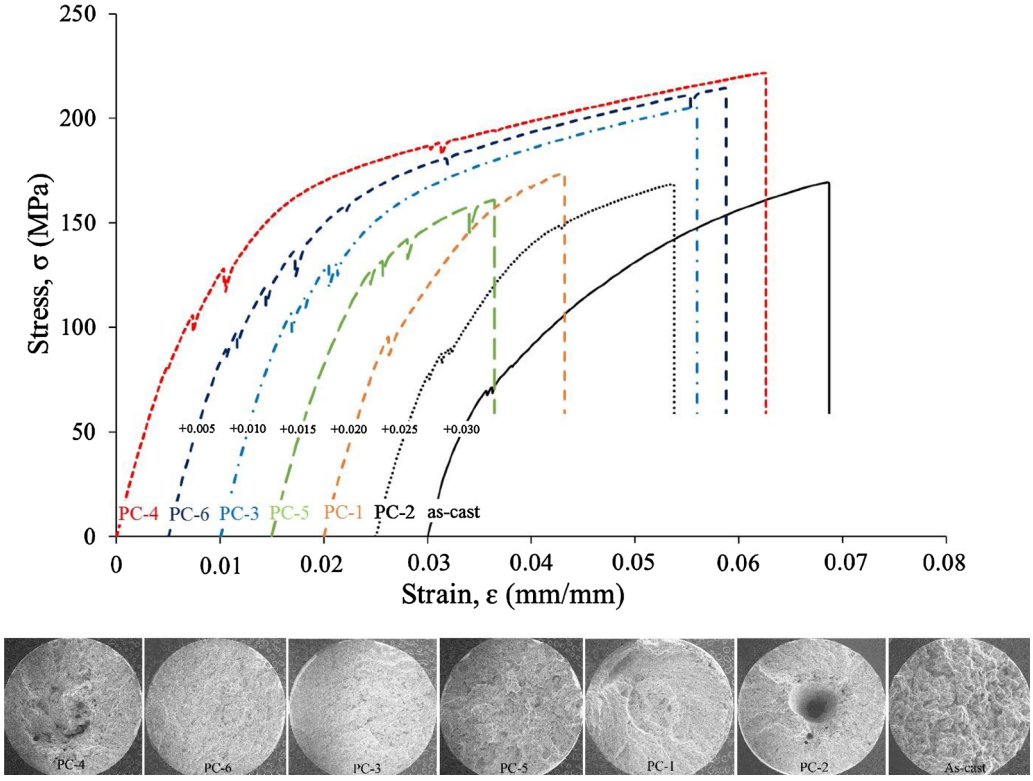

Fig. 4. Stress-strain curve and fracture surfaces of As-cast and pressure die casting samples.

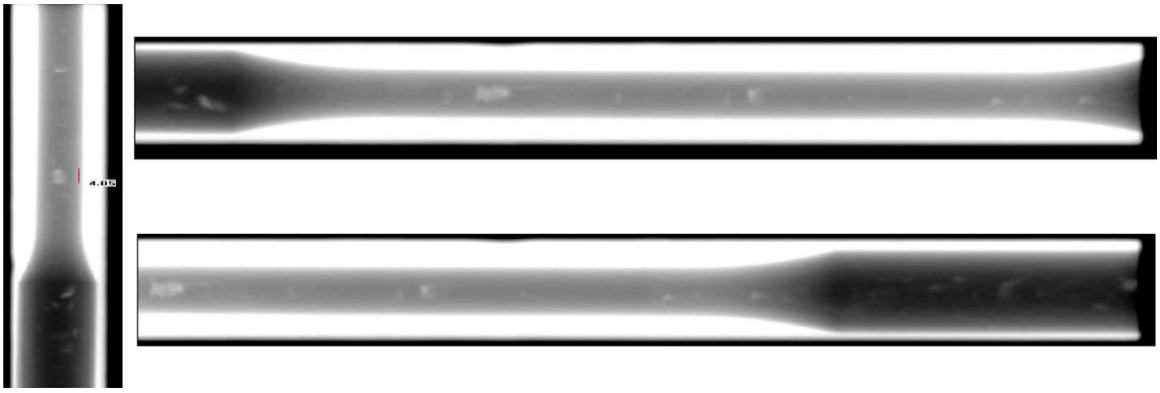

Fig. 5. Porosity images of a PC-5 sample taken by X-ray tomography.

explained for two reasons; the first is grain shrinkage. Grain size significantly affects the mechanical properties of metals. As the grain size decreases at room temperature, the yield limit, tensile strength, and stiffness generally increase. The effect of fine grain structure on the mechanical properties of a material at room temperature is mainly; strength (or hardness) and ductility, hence increased toughness. The second one is the formation of a second phase including Mg and Al in the microstructure which causes second-phase hardening. The proportions of the phases affect the properties of the alloy. In the PC-1, PC-2, and PC-5 samples, it was found that the amount of α-Mg phase was high when the grains were larger and the phase ratios were taken into consideration. A stable phase distribution is generally expected at temperatures above 650 °C. However, it was observed that the phase transformation was not as expected due to the higher gate speed of the PC-5 sample. High gate speed causes porosity in the structure due to a phenomenon which is called as jetting during molding. It can be said that viscosity of the solid solution decreases at temperatures above 650 °C and this provides to be mold filling more easily. With an appropriate pressure, the internal resistance of the mold is overcome and the porosity decreases. As a conclusion, it can be said that low gate speed is more appropriate both in terms of grain structure and phase ratio.

Although the PC-5 sample was produced at an appropriate temperature and pressure parameter, a low tensile strength was obtained. It

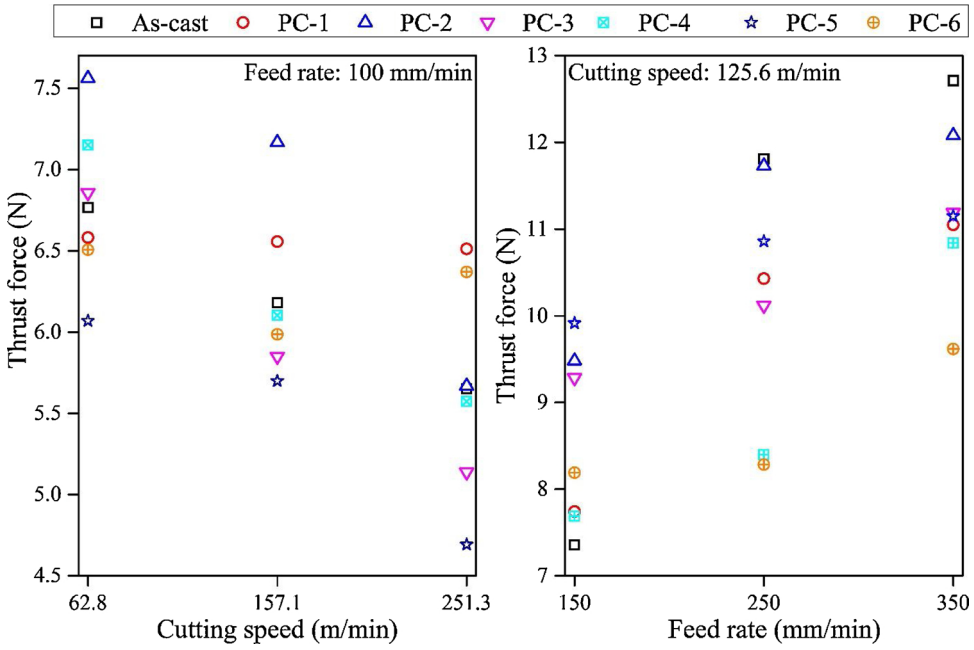

Fig. 6. Thrust force generation in the drilling of As-cast and pressure casting samples.

is thought that the reason for the lower tensile strength value compared to PC-4 and PC-6 was due to high gate speed (Table 3). In the manufacturing of the PC-5 sample, due to the high gate speed (60 m/s), porosities were formed by jetting (spraying). Due to these porosities, a lower tensile strength was obtained. The porosity formed in the PC-5 sample is shown in Fig. 5, which is obtained by X-ray tomography analysis.

3.3. Thrust force analysis

Thrust force affects tool wear, surface quality, vibration, the temperature of the cutting zone, and power consumption. Therefore, measuring the forces during the drilling process is important. Thrust force generated during drilling of As-cast and pressure die casting specimens using different cutting parameters are given in Fig. 6. The thrust force increased with increasing feed rate due to increasing uncut chip, shear area, and the energy required for cutting. On the other hand, the thrust force decreased with increasing cutting speed. This behavior was ascribed to the reduction of the contact area at the cutting tool-workpiece interface and the reduction of the specific cutting energy. Furthermore, with an increase in cutting speed, it is speculated that the cutting temperature increased and subsequently, material hardness was reduced. As a result, the thrust force also reduced [13]. The thrust force results from drilling seven different samples using three different cutting speeds (62.8, 157.1, and 251.3 m/min) varied between 4.6 N–7.5 N. Similarly, the thrust forces generated during drilling of these samples using three different feed rates (150, 250, and 350 mm/min) vary between 7.3 N–12.7 N. The feed rate had a greater influence on the developed thrust force than the cutting speed. A linear relationship could not be established between the thrust force and the samples because, during drilling, the drill may coincide with the existing casting porosity in the material. Besides, the chip squeeze during drilling affects the force results [28].

3.4. Tool wear analysis, Built-Up Edge (BUE) and Built-Up Layer (BUL) formation

Tool wear is a major factor that affects cutting force, temperature, exit burr, hole accuracy, and machined surface quality [29,30]. In this study, the flank wear of the cutting tools was measured since it is one of the most widely used wear criteria. The flank wear was measured with the help of a Keyence digital microscope (VHX-900 F). It was observed that the minimum wear (~ 27 μm) is formed in the drilling of the As-cast sample. Drilling of the PC-5 specimen resulted in approximately 45 μm wear as shown in Fig. 7a. The reason for the minimum tool wear formed in drilling PC-5 sample compared to the other pressure casting samples is that the hard intermetallic $Mg_{17}Al_{12}$ phase ratio is lower in this sample. In addition, cavities and porosities were formed in the sample since high gate speed was used in the manufacturing of this sample. It is thought that the wear on the tool is reduced due to these cavities/porosities. For high-speed drilling of PC-1 and PC-4 samples, approximately 55 μm of flank wear was measured. The maximum tool wear (approximately 73 μm) was measured in the drilling PC-6 sample (Fig. 7b). The second phases and grain size in the microstructure are an important factor affecting the mechanical properties of the alloy. Considering the microstructure of the PC-6 sample, the small size of the grains and the relatively high rates of hard intermetallic $Mg_{17}Al_{12}$ phase (Table 5) along the grain boundaries caused the mechanical properties and consequently the hardness of the material to be high (Table 6). The increase in mechanical properties resulting from changes in the microstructure caused a significant impact on the rate of wear in the drill. In addition, when the chips formed during the drilling of PC-6 sample

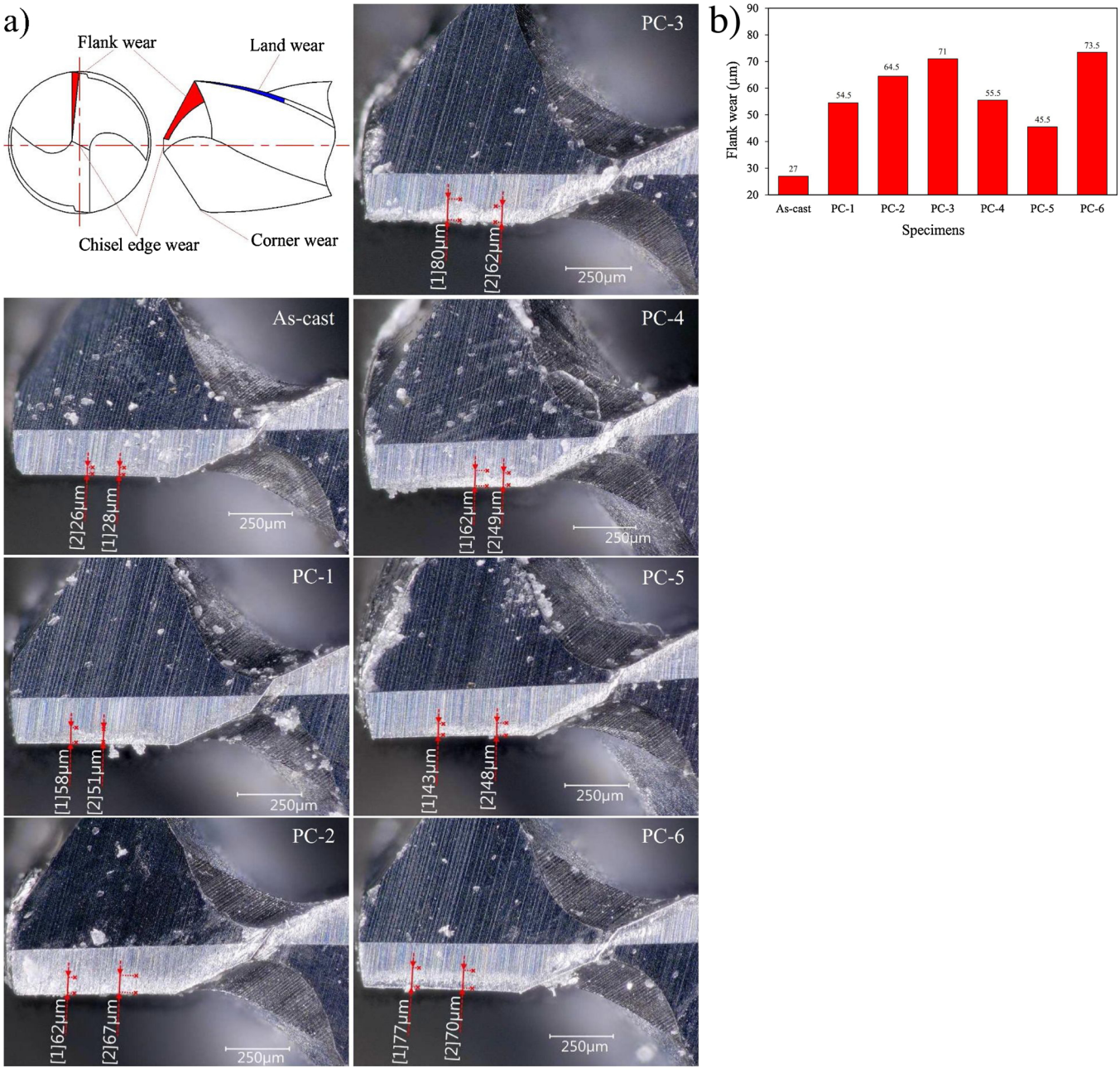

Fig. 7. a Flank wear formation in drilling of specimens. b Average flank wear as a function of specimens.

were examined (Fig. 11), it was seen that the chips formed as steady-state folded long ribbon type. Since it is difficult to remove this type of chip from the cutting zone, the formation of heat in the cutting zone increases due to friction, which phenomenon leads to an increase in tool wear. On the other hand, when taking into consideration the mechanical properties of the As-cast sample, low tensile strength and high ductility are thought to be the cause of the low level of wear on the cutting tool.

In the drilling of AZ91 alloys produced with different pressure casting parameters, BUE and BUL formation -due to the adherence of chip to the cutting tool- are shown in Fig. 8. When the figure is examined, in all samples, depending on the microstructure and mechanical properties of the specimens, different sized BUL extending from the margin region to the land region of the drill is formed. In addition, different sizes of BUE were observed in the cutting lip. In the drilling of PC-1, PC-2, and PC-5 samples, less BUE and BUL were formed in the cutting tool compared to other samples. When phase ratios in samples were examined as shown previously in Table 5, it was concluded that higher proportions of α-Mg phase were effective in BUE and BUL dimensions. The reason for the large amounts of BUE and BUL in PC-3,

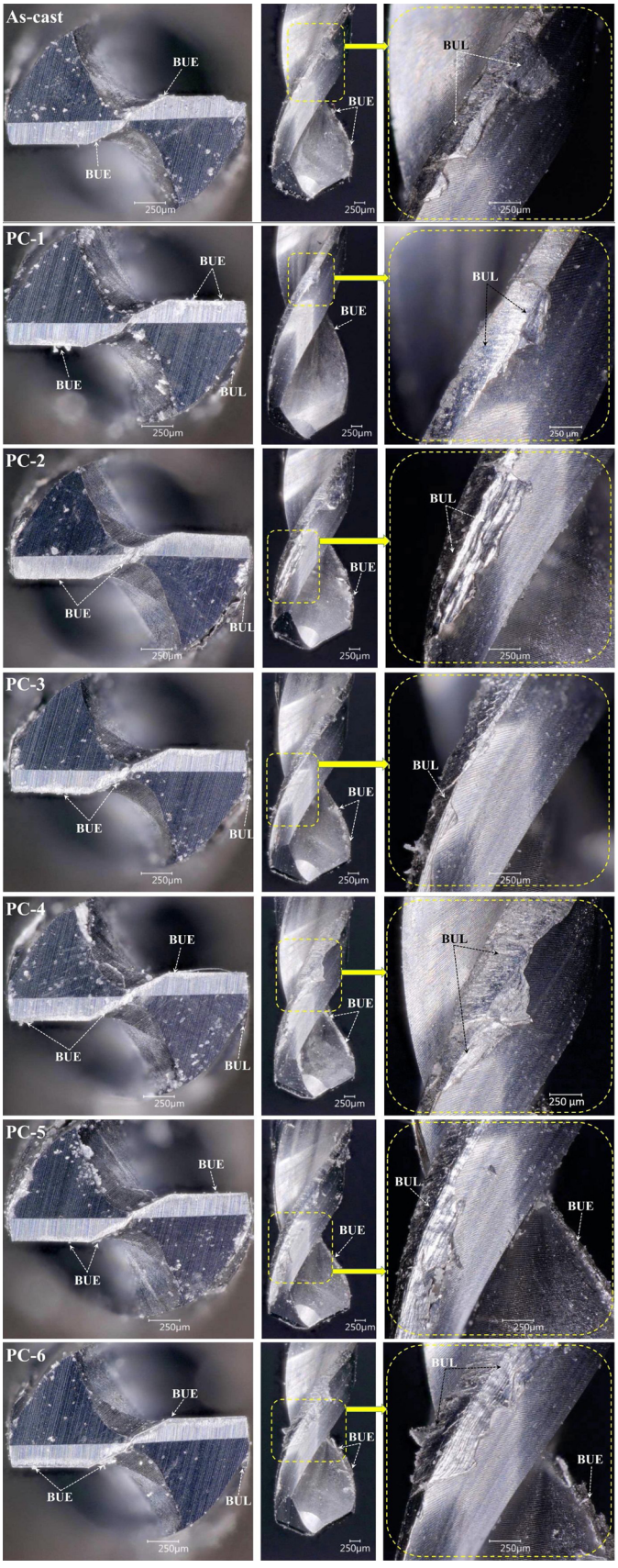

Fig. 8. BUE and BUL formation in drilling of AZ91 alloys.

PC-4, and PC-6 samples could be attributed to their high ductility and plastic deformation properties [31].

3.5. Surface topography

In industrial applications, surface finish is a crucial factor that affects the quality and performance of mechanical parts, as well as production costs. Much research has been carried out on minimizing flaws in the surface by machining various engineering materials with different cutting combinations [32]. In this study, in order to examine borehole surface topography, holes were cut into two parts from the axis. Roughness maps of the boreholes are shown in Fig. 9. Since the areal surface texture parameters (S_a, S_q, S_z, etc.) include an infinite number of profile surface texture parameters (R_a, R_q, R_z, etc.), 3D parameters (areal surface texture parameters) are better at describing the surface texture [33,34]. The values of S_a, S_z, S_q, S_{ku}, and S_{sk} for the drilled surface of different specimens are given in Table 7. Also, the roughness results as a function of casting and cutting parameters are presented as a bar chart with the standard deviation in Fig. 10. As can be shown in the figure, S_a decreased with increasing cutting speed. On the other hand, the surface quality deteriorated with increasing feed rate. This phenomenon is related to increasing heat generation and the cutting force required for drilling. The plastic deformation of the workpiece is proportional to the amount of heat generation in the workpiece and promotes roughness on the workpiece surface [35]. When the borehole surface of samples is compared, it is seen that the PC-2 sample has the worst surface among others and the surface of PC-1 and PC-6 samples also have a poor surface quality while PC-4, PC-5, and PC-3 samples have a somewhat better surface finish. The reason for the high surface roughness values observed in the PC-2 sample is due to the porosity caused by the high gate speed (60 m/s) used in the production phase of the sample. (A large porosity is seen in Fig. 4 (SEM images) for PC-2 sample). It is thought that the porosity in the material is responsible for high roughness values rather than the traces created by the drill during the drilling of the material. Consequently, the porosities not only reduce mechanical strength but also have a negative impact on machinability by reducing surface quality.

3.6. Chip morphology

The chip morphology that occurs in the drilling varies depending on the workpiece/cutting tool material, cutting tool geometry, coolant utilization, and cutting parameters. In general, chip formation in drilling can be classified into eight types: needle, powder, fan, short ribbon, short spiral cone, long ribbon, long spiral cone, and very long ribbon [36,37]. In this experimental study, three different types of chip were formed: fan, spiral cone, and long ribbon. Some of the micro and macro images of the obtained chips are given in Fig. 11.

When the chip shapes are examined in Fig. 11, it is seen that in drilling the As-cast sample, higher cutting speed and lower feed rate formed long ribbon chips, and as the feed rate decreased, the shape of the formed chip looked like a spiral cone. In drilling PC-1, PC-2, and PC-5 samples, fan-shaped chips were formed at 157.1 m/min cutting speed and low feed rates. The chip form turns to the spiral cone by decreasing cutting speed and increasing feed rate. PC-3, PC-4, and PC-6 samples were found to form long ribbon and spiral cone chips. The fan-shaped chip form starts with a spiral, but the drill does not bend sufficiently to flow along with the flutes and thus breaks before a full cycle can occur. When the stress-strain graphs of PC-1, PC-2, and PC-5 samples shown previously in Fig. 4 were examined, it was found that their plastic deformation capabilities were lower compared to other samples. Due to the mechanical properties of these samples, it can be said that the chip

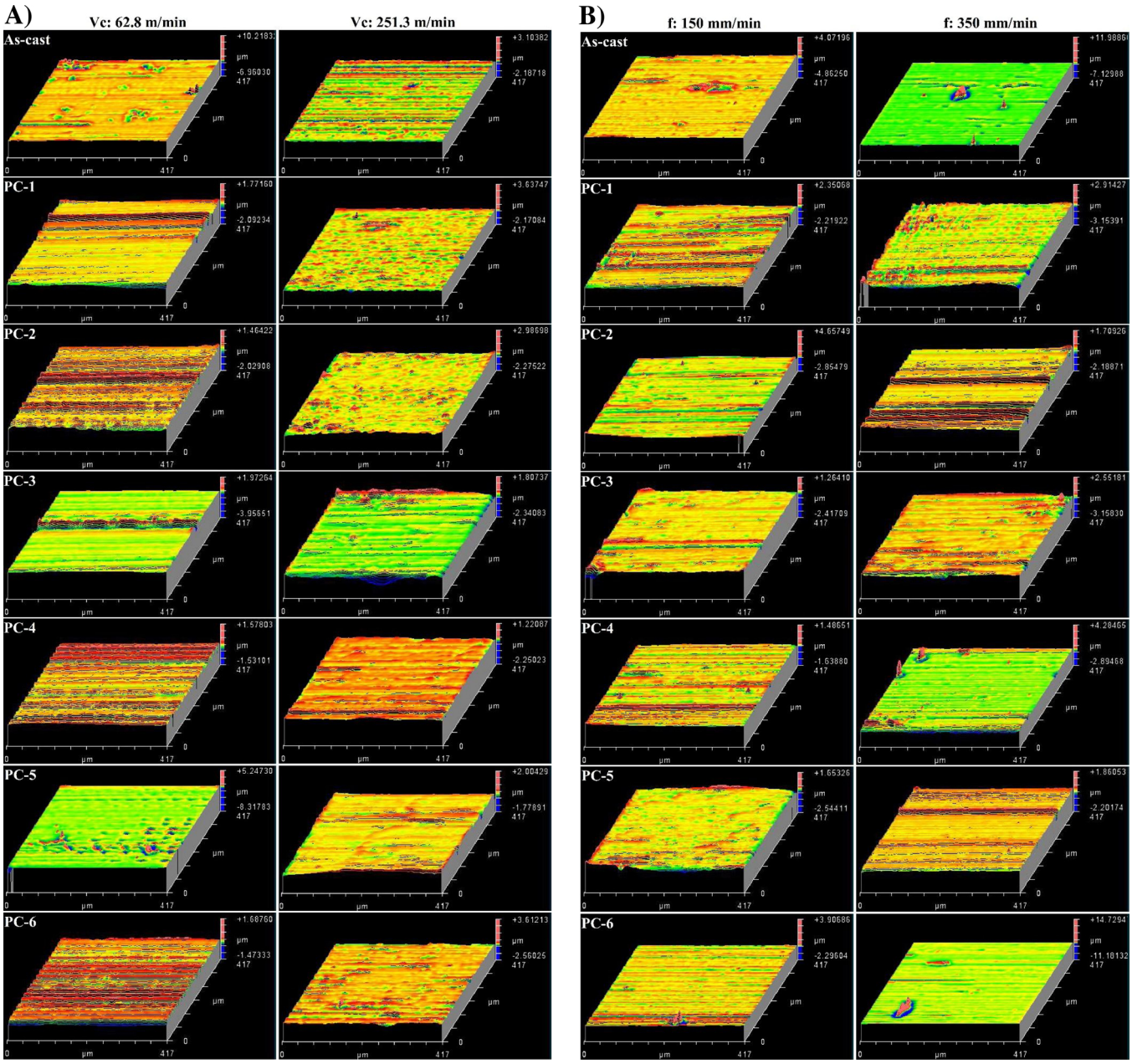

Fig. 9. a Borehole surface roughness maps of specimens depending on cutting speed. b Borehole surface roughness maps of specimens depending on feed rate.

becomes brittle and broken in the drill flute by the effect of the severe plastic deformation and thus fan-shaped chip are formed. Furthermore, when the microstructures of PC-1, PC-2, and PC-5 samples were examined, it was observed that the α-Mg phase ratios of these samples were higher than the other samples as shown previously in Table 5. It was also observed that phase ratios of α-Mg-$Mg_{17}Al_{12}$ formed in different ratios due to production parameters were effective in chip morphology in the drilling process of AZ91 alloys. Due to the high ductility and plastic deformation ability of As-cast, PC-3, PC-4, and PC-6 samples (Fig. 4), chips are easily curled in flute and formed as long ribbon and spiral cone. As stated in the literature, the fan-shaped chip is considered the most ideal chip shape in terms of machinability due to the easier chip evacuation [37,38].

In all of the cutting parameters used in the experiments, the free surface of the chips showed lamella structures perpendicular to the flow direction of the chip and extending along the width of the chip (Fig. 11). This lamella structure on the free surface of the chips is a result of the presence of shear localization [39,40]. When the shear stress exceeds the critical level, catastrophic failure occurs in the area above the primary deformation zone due to high plastic deformation. This damage mechanism leads to splits that cause the formation of new coverslips. The size of the segmented structure formed on the free

Table 7
Borehole surface roughness values of As-cast and pressure casting samples.

Specimen	Roughness metric	62.8 m/min	157.1 m/min	251.3 m/min	150 mm/min	250 mm/min	350 mm/min
As-cast	S_a (μm)	0.096	0.081	0.062	0.066	0.073	0.098
	S_z (μm)	2.063	1.933	0.983	1.795	1.223	3.663
	S_q (μm)	0.174	0.131	0.08	0.12	0.114	0.213
	S_{ku} (μm)	38.12	17.91	4.32	39.01	21.35	63.42
	S_{sk} (μm)	−0.35	−0.55	−0.51	−3.19	−2.47	3.55
PC-1	S_a (μm)	0.106	0.093	0.052	0.087	0.092	0.1
	S_z (μm)	1.07	1.113	0.926	1.083	1.547	1.568
	S_q (μm)	0.182	0.134	0.074	0.117	0.157	0.143
	S_{ku} (μm)	9.154	6.23	11.63	4.73	16.56	7.79
	S_{sk} (μm)	−0.42	−0.25	−0.86	−0.67	−0.39	−0.67
PC-2	S_a (μm)	0.13	0.107	0.068	0.065	0.1	0.131
	S_z (μm)	0.984	1.98	1.162	1.184	1.538	1.133
	S_q (μm)	0.172	0.200	0.103	0.094	0.144	0.184
	S_{ku} (μm)	4.99	7.71	11.44	10.72	9.07	5.10
	S_{sk} (μm)	−0.64	0.37	−1.11	−0.34	0.55	−0.59
PC-3	S_a (μm)	0.086	0.079	0.079	0.048	0.061	0.088
	S_z (μm)	1.206	1.04	1.076	0.955	0.705	1.244
	S_q (μm)	0.141	0.109	0.116	0.078	0.083	0.132
	S_{ku} (μm)	9.95	5.83	11.20	14.19	5.32	7.92
	S_{sk} (μm)	−0.71	−0.74	−0.49	−1.61	−0.18	−1.25
PC-4	S_a (μm)	0.117	0.062	0.051	0.043	0.073	0.079
	S_z (μm)	0.723	1.212	0.789	0.575	0.966	2.067
	S_q (μm)	0.144	0.089	0.077	0.059	0.100	0.135
	S_{ku} (μm)	2.96	22.52	12.40	6.06	5.30	32.91
	S_{sk} (μm)	−0.31	−1.39	−1.96	−0.69	−0.32	1.85
PC-5	S_a (μm)	0.078	0.068	0.067	0.055	0.063	0.081
	S_z (μm)	2.308	1.214	0.753	0.981	0.684	0.862
	S_q (μm)	0.148	0.102	0.103	0.087	0.087	0.128
	S_{ku} (μm)	37.85	11.68	10.24	13.31	4.90	9.43
	S_{sk} (μm)	−1.94	−1.14	−1.14	−1.08	−0.23	−1.55
PC-6	S_a (μm)	0.109	0.107	0.069	0.047	0.066	0.081
	S_z (μm)	0.636	1.074	1.249	0.888	0.66	2.698
	S_q (μm)	0.130	0.227	0.103	0.077	0.133	0.236
	S_{ku} (μm)	2.42	7.09	11.09	6.50	12.29	20.95
	S_{sk} (μm)	−0.47	−0.47	−1.08	0.36	−2.78	0.82

surface of chips varies depending on the microstructure, mechanical properties of the material, and cutting parameters. In Fig. 11, stresses caused by high cutting forces at low cutting speeds lead to the lamella structure on the free surfaces of the formed chip to be relatively thin and smooth. This phenomenon can be explained by the occurrence of crack initiations in the area above the primary deformation zone as a result of shear localization caused by the increased stress at relatively low cutting speeds [41]. As cutting speed increases, the reduction in cutting forces and the reduction of the stresses between the tool/material result in a coarser lamella structure. When the free surfaces of the chip occurred at different feed rates were examined, it was observed that the size of the lamella and the thickness of the undeformed chip increased as the feed rate increased. However, the effect of the feed rate on the lamella structure was found to have a lesser effect than the effect of the cutting speed. Besides, it has been observed that all of the chips have corner bands in the form of sharp saw teeth.

When the chips formed in drilling AZ91 alloys produced with different pressure casting parameters were evaluated in terms of material properties, it was seen that there was no significant change in the dimensions of the lamella formed on the free surface of the chip. However, compared to the As-cast sample, it was noticed that the lamella structure on the free surfaces of the chips produced by the pressure casting method was coarser. When the microstructure of the samples produced by the pressure casting method is examined, it is seen that they have finer grain structures than As-cast. On the other hand, there is no significant difference between the microstructures of the samples produced by the pressure casting method with different casting parameters. This difference in grain structure also affects chip morphology and is thought to be the reason for the difference in the lamella structure formed on the free surface. A significant amount of microstructural deformation occurs in the primary shear region. The grains extend into thin strips along the shear direction. This phenomenon may be due to the dynamic recrystallization of grains formation and thermal softening effect. The friction between the back surface of the chip and the tool surface produces a higher deformation temperature. The grain boundaries increase the mobility, the higher grain boundaries in the pressure casting samples having small grain structure significantly alter the chip morphology.

The back surfaces of the chips in different shapes as a result of drilling operations are shown in Fig. 11. The smooth surfaces on the back surfaces of the chips are caused by high contact and shear stress on the rake face [42]. However, an irregular wavy surface on the back surfaces of the chips is remarkable. Random voids and traces of sporadic deterioration were found on the back of the chips (Fig. 11). It was determined that the void formed on the back surface of the chips had no melting traces due to the high heat generated during the drilling

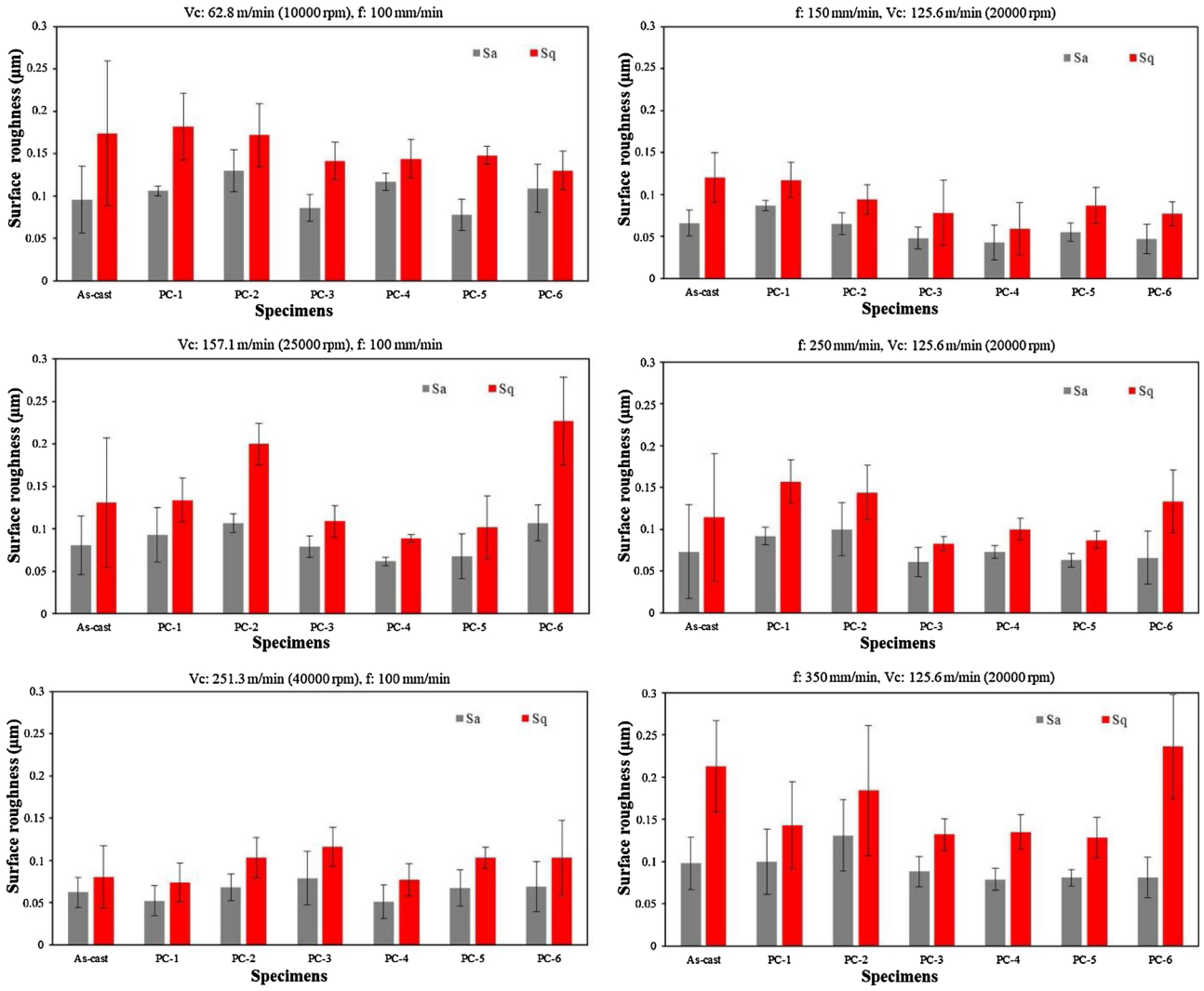

Fig. 10. Roughness results as a function of casting and cutting parameters.

process and the random casting gaps in the drilled material affected on the chip surface. The chip tended to adhere to the tool surface due to high friction between the tool surface and the chip surface. Moreover, the BUE is harder than the work material due to its plastic deformation effect and can change tool geometry by acting as a cutting edge. Materials adhering to the tool chip face cause an irregular chip flow pattern on the back surface of the chip.

3.7. Burr analysis

The burr formation in the drilling process is the unwanted external projections that occur in the exit area of the hole and it is formed in three different (uniform, transient, and crown) shapes depending on the properties of the workpiece material, cutting parameters, cutting tool geometry, cutting forces and chip formation during cutting [43] as shown in Fig. 12. After many machining operations, burrs are formed on the workpiece, the size of the burrs can be measured using different methods [44–46]. In this study, the burr size was not measured. Only, the formed burrs were monitored and categorized depending on casting and cutting parameters.

The uniform burr is formed in a small size around the hole exit. Generally, a burr is formed during the process, which can be removed from the part, or can be easily removed later. The uniform burr is occurred by a first fracture in which the compression stress is applied to the material by the chisel edge in the center of the hole. As the cutting tool proceeds, the plastic deformation area enlarges from the center of the hole to the edges of the drill and a second break occurs around the hole (Fig. 12a). The transient burr has a shape between uniform and crown burr. Fractures occurred in the material at the hole exit are formed almost simultaneously in the center and around the hole. Therefore, first occurs in the form of a burr crown and then in a uniform form (Fig. 12b). Crown burr and large sizes around the exit hole are formed irregularly. The plastic deformation in the center of the bore increases with increasing feed rate and thrust force (Fig. 12c).

The images of the burrs formed around the hole exit as a result of drilling of AZ91 alloys produced in different casting parameters are given in Fig. 13. As it appears in the figure, uniform and transient burr formation were observed in all samples depending on cutting parameters but crown burr formation was not observed. It was observed that there was no significant change in the burr amount of PC-3, PC-4, and

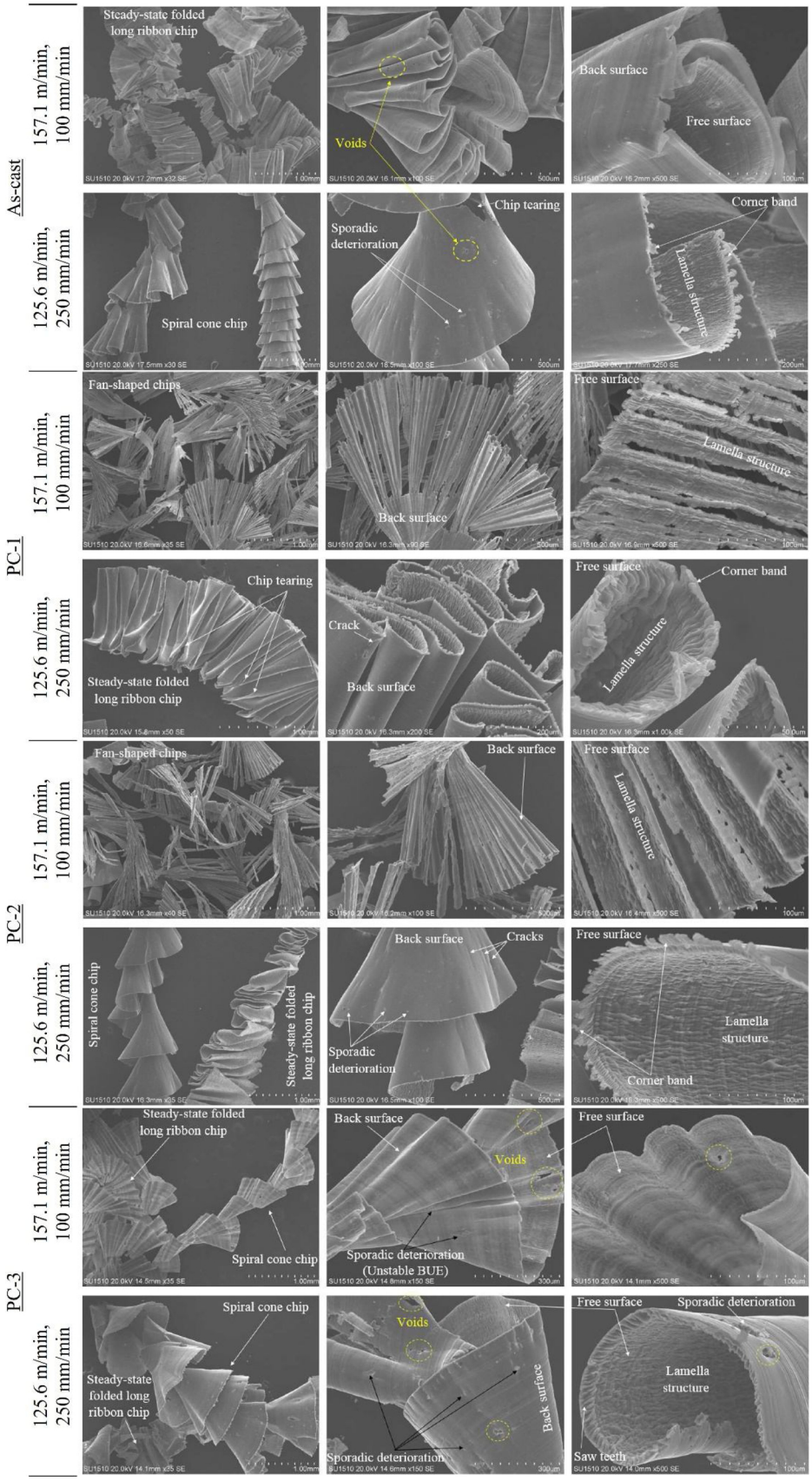

Fig. 11. Chip formation in drilling of AZ91 alloy.

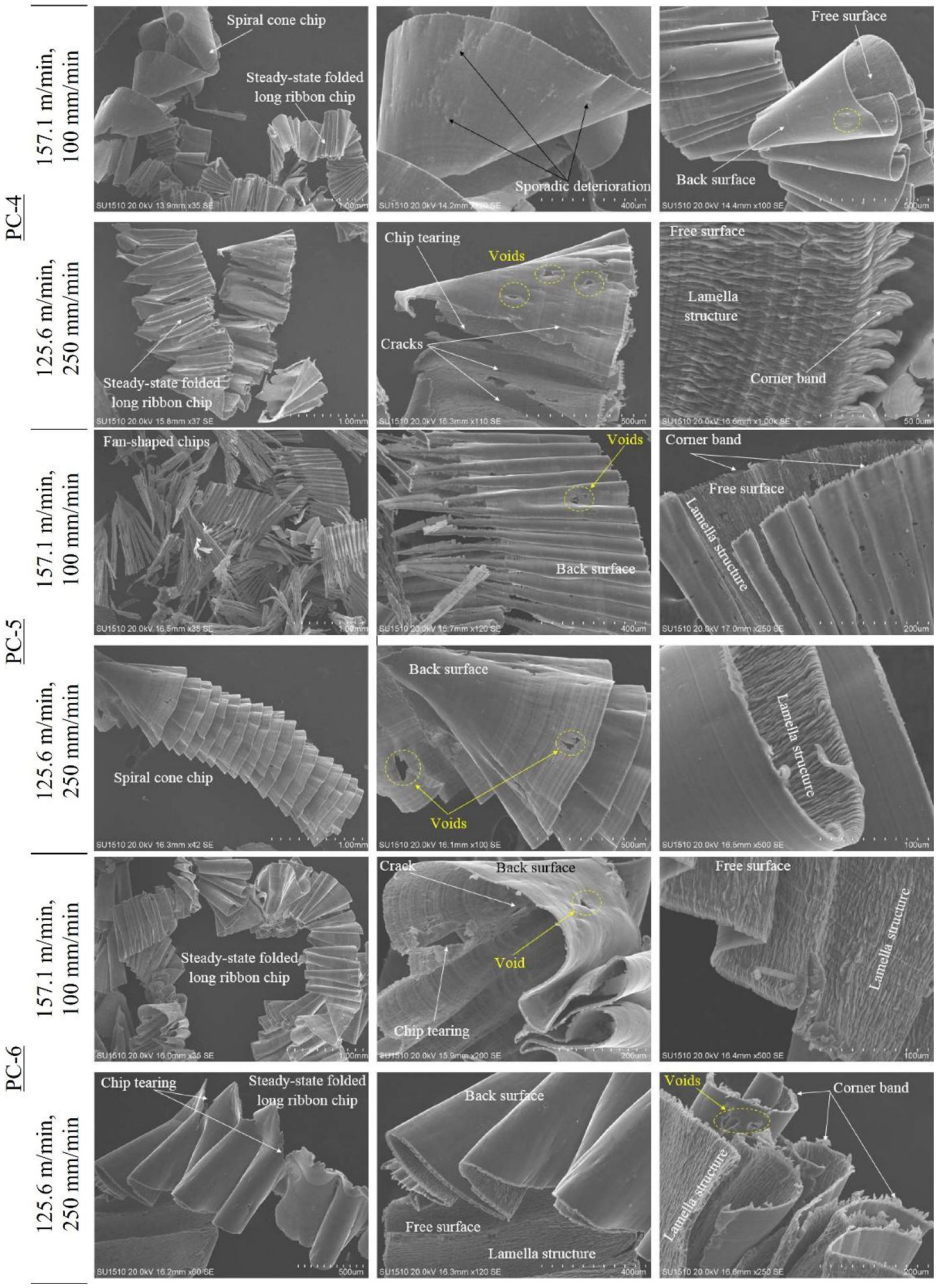

Fig. 11. (*continued*)

PC-6 samples with increasing feed rate, but burr formation decreased in As-cast, PC-1, PC-2, and PC-5 samples. The probable reason for this is thought to be a significant increase in cutting forces (Fig. 6) as the feed rate increases. It can be said that the stress formed due to high cutting forces with the increase of the feed rate prevents the formation of large burrs by breaking the chips at the exit of the hole. However, it was found that the amount of burr tended to increase as the cutting speed increased in all samples. Transient burr was observed in all samples at the highest cutting speed, while uniform burr was observed at the lowest cutting speed except As-cast and PC-2 samples. Depending on the increase in cutting speeds, a significant reduction in the thrust force occurred, especially in the drilling of the PC-2 sample (Fig. 6). Also, considering the mechanical properties of the PC-2 sample, it is seen that the yield strength is lower compared to other samples (Table 6). With the decrease in the cutting forces, the stress in the cutting area decreases as well. The low stress that occurs at higher cutting speeds in the drilling PC-2 sample may not be sufficient to break the burrs at the exit of the hole and remove it from the zone. This phenomenon is thought to lead to larger burr formation, especially at high-speed cutting. When drilling the As-cast sample, a transient burr was formed at the hole exit in all cutting parameters (Fig. 13). Due to the coarse-grained structure of the As-cast sample, (Table 5), burr formation is adversely affected. On the other hand, in PC-6 sample, the reason for the formation of less burr can be attributed to finer grain structure and

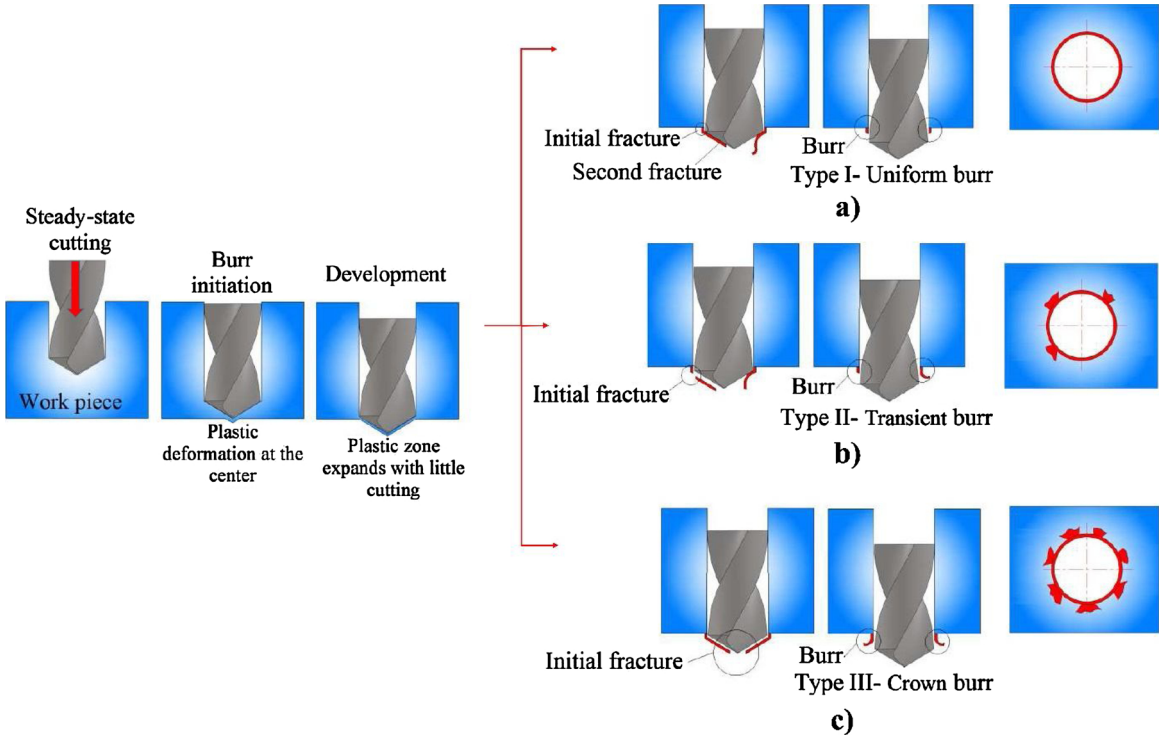

Fig. 12. Burr formation mechanism during drilling.

higher intermetallic $Mg_{17}Al_{12}$ phase (Table 5).

Increased stresses in the cutting zone due to the cutting parameters (particularly feed rate (Fig. 6) caused the plastic deformation to intensify and expand from the center of the hole to the edges as the plastic deformation in the center of the hole started early and proceeded to the exit of the drill. When the mechanical properties of PC-1, PC-2, and PC-5 samples are examined, it is observed that their yield strength and plastic deformation ability are generally low (Fig. 4). The low plastic deformation ability and strength of these samples showed a relatively brittle behavior due to the increasing stresses and caused the burr to be broken early and removed from the hole exit and therefore decreased in size. The tension generated by the high shear forces at high feed rates is sufficient to break the material causing burr formation at the hole exit.

4. Conclusions

High-speed drilling of casted AZ91 Mg alloys produced using cold die casting parameters such as casting temperature, molding pressure, and gate speed, and different cutting parameters (cutting speed and feed rate) were investigated. The aim was to study the effects of different casting parameters on microstructure, mechanical properties and machinability characteristics (thrust force, tool wear, built-up edge, built-up layer formation, surface topography, chip morphology, and burr formation). The results obtained from the experimental study are given below.

- As a result of the microstructure examination of the samples produced with different pressure casting parameters and As-cast, the ASTM grain size of the As-cast sample was 5.5 while the ASTM grain sizes of the pressure casting samples were between 9 − 10. There was a decrease in the grain structure of the samples produced by the pressure casting method.
- It is seen that the samples produced with suitable casting parameters (casting temperature above 650 °C, 800 − 1000 bar molding pressure, and 30 − 45 m/s gate speed) showed better mechanical properties by providing a finer grain structure. On the other hand, porosities in samples produced with high gate speed lower mechanical properties.
- The thrust forces generated in drilling the samples using three different cutting speeds range from 4.6 N to 7.5 N. Similarly, the thrust forces vary between 7.3 N–12.7 N depending on different feed rates. In the formation of thrust force, the feed rate is more effective than the cutting speed. Since the samples were not homogeneous, a linear relationship between the thrust force and the samples could not be established.
- The highest flank wear occurred in the drilling of PC-6 sample (73 μm), while the least flank wear occurred in the drilling of the As-cast sample (27 μm).
- In borehole surface topography comparison, the worst surface was obtained in PC-2 and the best surface was obtained in PC-3, PC-4, and PC-5 samples.
- Casting and cutting parameters directly affect chip formation. The fan, spiral cone, and long ribbon chips were seen depending on cutting parameters.
- Uniform and transient burrs were formed at the hole exits, but crown burr formation was not observed. The most burr was formed in the As-cast sample, while the least burr was in the PC-6 sample.

Declaration of Competing Interest

The authors declare that there are no conflicts of interest.

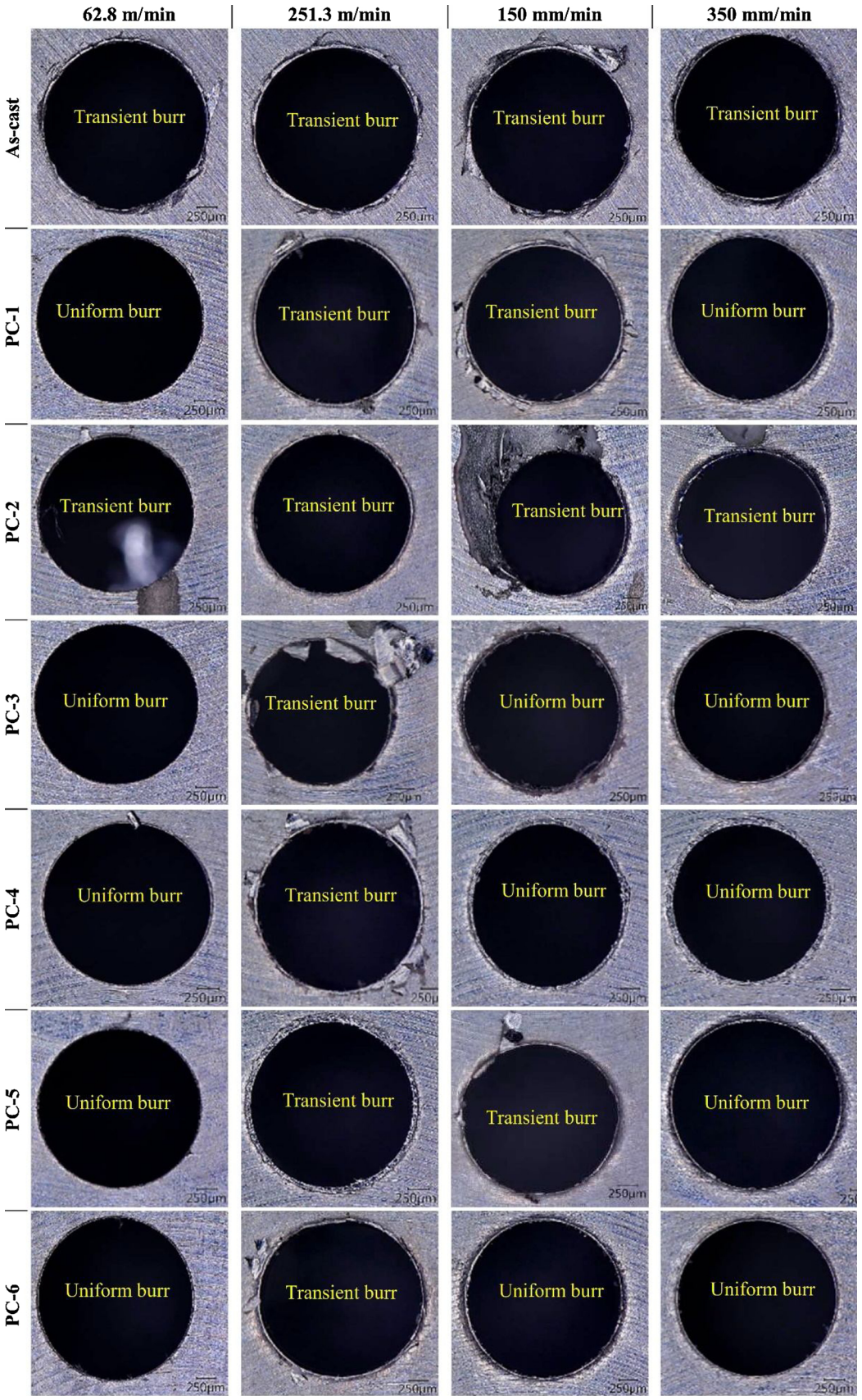

Fig. 13. Burr formation depending on casting and cutting parameters.

References

[1] Bhowmick S, Lukitsch MJ, Alpas AT. Dry and minimum quantity lubrication drilling of cast magnesium alloy (AM60). Int J Mach Tools Manuf 2010;50:444–57.
[2] Dahle AK, Sannes S, John DHSt, Westengen H. Formation of defect bands in high pressure die cast magnesium alloys. J Light Met 2001;1:99–103.
[3] Pu Z, Outeiro JC, Batista AC, Dillon OW, Puleo DA, Jawahir IS. Enhanced surface integrity of AZ31B Mg alloy by cryogenic machining towards improved functional performance of machined components. Int J Mach Tools Manuf 2012;56:17–27.
[4] Şahbaz M, Kaya H, Kentli A. A new severe plastic deformation method: thin-walled open channel angular pressing (TWO-CAP). Int J Adv Manuf Technol 2020;106:1487–96.
[5] Kulekci MK. Magnesium and its alloys applications in automotive industry. Int J Adv Manuf Technol 2008;39:851–65.
[6] Zeng X, Wang Y, Ding W, Luo AA, Sachdev AK. Effect of strontium on the microstructure, mechanical properties, and fracture behavior of AZ31 magnesium alloy. Metall Mater Trans A 2006;37:1333–41.
[7] Koklu U, Coban H. Effect of dipped cryogenic approach on thrust force, temperature, tool wear and chip formation in drilling of AZ31 magnesium alloy. J Mater Res Technol 2020. Article in Press.
[8] Dinesh S, Senthilkumar V, Asokan P, Arulkirubakaran D. Effect of cryogenic cooling on machinability and surface quality of bio-degradable ZK60 Mg alloy. Mater Des 2015;87:1030–6.
[9] Balout B, Songmene V, Masounave J. An experimental study of dust generation during dry drilling of pre-cooled and pre-heated workpiece materials. J Manuf Process 2007;9:23–34.
[10] Berzosa F, de Agustina B, Rubio E. Tool selection in drilling of magnesium UNSM11917 pieces under dry and mql conditions based on surface roughness. Procedia Eng 2017;184:117–27.
[11] Bhowmick S, Alpas A. The role of diamond-like carbon coated drills on minimum quantity lubrication drilling of magnesium alloys. Surf Coat Technol 2011;205:5302–11.
[12] Kayir Y. Optimization of the cutting parameters for drilling magnesium alloy AZ 91. Mater Test 2014;56:47–53.
[13] Koklu U, Morkavuk S, Urtekin L. Effects of the drill flute number on drilling of a casted AZ91 magnesium alloy. Mater Test 2019;61:260–6.
[14] Sunil BR, Ganesh K, Pavan P, Vadapalli G, Swarnalatha C, Swapna P, et al. Effect of aluminum content on machining characteristics of AZ31 and AZ91 magnesium alloys during drilling. J Magnes Alloy 2016;4:15–21.
[15] Wang J, Liu Y, An J, Wang L. Wear mechanism map of uncoated HSS tools during drilling die-cast magnesium alloy. Wear 2008;265:685–91.
[16] Buldum B, Eşme U, Kemal Külekci M, Şik A, Kazançoğlu Y. Use of grey-taguchi method for the optimization of oblique turning process of AZ91D magnesium alloy. Mater Test 2012;54:779–85.
[17] Carou D, Rubio EM, Lauro CH, Davim JP. Experimental investigation on surface finish during intermittent turning of UNS M11917 magnesium alloy under dry and near dry machining conditions. Measurement 2014;56:136–54.
[18] Chowdary S, Dumpala R, Kondaiah V. Influence of heat treatment on the machinability and corrosion behavior of AZ91 Mg alloy. J Magnes Alloy 2018;6:52–8.
[19] Viswanathan R, Ramesh S, Subburam V. Measurement and optimization of performance characteristics in turning of Mg alloy under dry and MQL conditions. Measurement 2018;120:107–13.
[20] Shi K, Zhang D, Ren J. Optimization of process parameters for surface roughness and microhardness in dry milling of magnesium alloy using Taguchi with grey relational analysis. Int J Adv Manuf Technol 2015;81:645–51.
[21] Shi K, Zhang D, Ren J, Yao C, Huang X. Effect of cutting parameters on machinability characteristics in milling of magnesium alloy with carbide tool. Adv Mech Eng 2016;8:1–9.
[22] Fang FZ, Lee LC, Liu XD. Mean flank temperature measurement in high speed dry cutting of magnesium alloy. J Mater Process Technol 2005;167:119–23.
[23] Kuczmaszewski J, Zagórski I, Dziubinska A. Investigation of ignition temperature, time to ignition and chip morphology after the high-speed dry milling of magnesium alloys. Aircr Eng Aerosp Technol: Int J 2016;88:389–96.
[24] Kuczmaszewski J, Zagórski I, Zgórniak P. Thermographic study of chip temperature in high-speed dry milling magnesium alloys. Manag Prod Eng Rev 2016;7:86–92.
[25] Zagórski I, Kuczmaszewski J. The study of cutting forces and their amplitudes during high-speed dry milling magnesium alloys. Adv Sci Technol Res J 2013;7:61–6.
[26] Ruslan MS, Othman K, Ghani JA, Kassim MS, Haron CHC. Surface roughness of magnesium alloy AZ91D in high speed milling. J Teknol 2016;78:115–9.
[27] Shi K, Ren J, Zhang D, Zhai Z, Huang X. Tool wear behaviors and its effect on machinability in dry high-speed milling of magnesium alloy. Int J Adv Manuf Technol 2017;90:3265–73.
[28] Cedergren S, Simeone A, Wretland A. Adaptive process monitoring of holemaking operations. 2020.
[29] Uludağ M, Yazman Ş, Gemi L, Bakircioğlu B, Erzi E, Dispinar D. Relationship between machinability, microstructure, and mechanical properties of Al-7Si alloy. J Test Eval 2018;46:2592–603.
[30] Yazman Ş, Gemi L, Uludağ M, Akdemır A, Uyaner M, Dişpinar D. Correlation between machinability and chip morphology of austempered ductile Iron. J Test Eval 2017;46:1012–21.
[31] Dhar NR, Islam MW, Islam S, Mithu MAH. The influence of minimum quantity of lubrication (MQL) on cutting temperature, chip and dimensional accuracy in turning AISI-1040 steel. J Mater Process Technol 2006;171:93–9.
[32] Koklu U, Basmaci G. Evaluation of tool path strategy and cooling condition effects on the cutting force and surface quality in micromilling operations. Metals 2017;7:426.
[33] Kakaboura A, Fragouli M, Rahiotis C, Silikas N. Evaluation of surface characteristics of dental composites using profilometry, scanning electron, atomic force microscopy and gloss-meter. J Mater Sci Mater Med 2007;18:155–63.
[34] Rudzitis J, Bulaha N, Lungevics J, Linins O, Berzins K. Theoretical analysis of spacing parameters of anisotropic 3D surface roughness. Latv J Phys Tech Sci 2017;54:55–63.
[35] Basavarajappa S, Suresh R, Gaitonde V, Samuel G. Analysis of cutting forces and surface roughness in hard turning of AISI 4340 using multilayer coated carbide tool. Int J Mach Mach Mater 2014;16:169–85.
[36] Boothroyd G. Fundamentals of metal machining and machine tools. Crc Press; 1988.
[37] Bakkal M, Shih AJ, McSpadden SB, Liu C, Scattergood RO. Light emission, chip morphology, and burr formation in drilling the bulk metallic glass. Int J Mach Tools Manuf 2005;45:741–52.
[38] Batzer S, Haan D, Rao P, Olson W, Sutherland J. Chip morphology and hole surface texture in the drilling of cast aluminum alloys. J Mater Process Technol 1998;79:72–8.
[39] Black JT. On the fundamental mechanism of large strain plastic deformation: electron microscopy of metal cutting chips. J Eng Ind 1971;93:507–26.
[40] Farid AA, Sharif S, Idris MH. Chip morphology study in high speed drilling of Al–Si alloy. Int J Adv Manuf Technol 2011;57:555–64.
[41] Van Luttervelt C, Pekelharing A. The split shear zone-mechanism of chip segmentation. CIRP Ann Manuf Technol 1977;25:33–7.
[42] Sun J, Guo Y. A new multi-view approach to characterize 3D chip morphology and properties in end milling titanium Ti–6Al–4V. Int J Mach Tools Manuf 2008;48:1486–94.
[43] Costa ES, Silva MBd, Machado AR. Burr produced on the drilling process as a function of tool wear and lubricant-coolant conditions. J Braz Soc Mech Sci Eng 2009;31:57–63.
[44] Matuszak J, Kłonica M, Zagórski I. Measurements of forces and selected surface layer properties of AW-7075 aluminum alloy used in the aviation industry after abrasive machining. Materials 2019;12:3707.
[45] Matuszak J, Zaleski K. Edge states after wire brushing of magnesium alloys. Aircr Eng Aerosp Technol: Int J 2014;86:328–35.
[46] Matuszak J, Zaleski K. Analysis of deburring effectiveness and surface layer properties around edges of workpieces made of 7075 aluminium alloy. Aircr Eng Aerosp Technol 2018;90:515–23.